Hydraulic transients in straight and coil pipe rigs

David Ferras[1,2], Pedro A. Manso[2], Anton J. Schleiss[2] and Dídia I.C. Covas[1]

[1] Civil Engineering Research and Innovation for Sustainability (CEris), Instituto Superior Técnico, Universidade de Lisboa (Portugal)
[2] Laboratory of Hydraulic Constructions (LCH), École Polytechnique Fédérale de Lausanne (Switzerland)

ABSTRACT

Transient pressure waves in real pipe systems are affected by several phenomena not accounted for in the classic waterhammer theory. Damping mechanisms are differently manifested according to the material, configuration and existing features of pipe systems. The identification of dominant cause-effect relationships are major challenges in today's research for better understanding the physics of the phenomena, being able to mathematically describing them, and carrying out a successful diagnosis of existing problems. This paper aims at reporting observed transient pressure waves in different pipe rigs and at discussing the respective principal damping mechanisms associated to fluid-structure interaction, friction, and material retarded response. Discussion highlights differences in the response of each system in terms of wave damping, shape and timing.

Key words: transient data, fluid-structure interaction, hysteresis, viscoelasticity, waterhammer.

NOTATION

a	wave celerity (m/s)
D	inner pipe diameter (m)
E	Young's modulus of elasticity (Pa)
e	pipe-wall thickness (m)
g	gravity acceleration (m/s^2)
H	piezometric head (m)
H_0	piezometric head during the initial steady state (m)
H_{max}	maximum piezometric head during the transient state (m)
H_{min}	minimum piezometric head during the transient state (m)
L	pipe length (m)
p	fluid pressure (Pa)
R	pipe coil radius (m)
r	inner pipe radius (m)
Re	Reynolds number (-)
Re_0	Reynolds number at initial steady state (-)
T	wave period (s)
t_{valve}	valve effective closing time (s)
V	section-averaged velocity of the flow (m/s)
V_0	section-averaged velocity of the flow during the initial steady state (m/s)
ΔH_{JK}	Joukowsky overpressure (m)
ε_c	pipe-wall circumferential strain (-)

μ Poisson ratio (-)
σ_c pipe-wall circumferential stress (Pa)

1 INTRODUCTION

Classical waterhammer theory considers several simplifications that frequently make the results of numerical simulations significantly differ from physical evidence observed both in controlled laboratory conditions and in the field. Some of these assumptions are (Chaudhry, 2014): 1D flow, steady friction, one-phase flow, uniform pipe geometry, no direct interaction between the fluid and its containing structure, linear-elastic behaviour of the pipe-wall and neither leaks nor blockages in the system.

The expertise of the modeller becomes crucial when add-ons are to be included into the classic waterhammer model. Phenomena such as *unsteady friction, cavitation, trapped air, fluid-structure interaction, pipe-wall viscoelasticity, leaks and blockages,* affect transient pressure wave amplitude, shape and timing. Engineers should attempt to identify and to evaluate the influence of these mechanisms in order to decide whether to include or to neglect them. Firstly, these phenomena are not included in standard waterhammer software packages and, secondly, these are often "hidden" in real systems (Bergant *et al.*, 2008).

Frequently, the referred damping phenomena have been tackled by researchers one at a time. Nevertheless, several examples can be found in literature of authors combining damping mechanisms either in experimental or numerical analyses, such us: Krause *et al.* (1977) or Williams (1977) who carried out experiments in plastic and metallic pipes, Weijde (1985); Walker & Phillips (1977) or Stuckenbruck & Wiggert (1986) who designed numerical models taking into account fluid-structure interaction and pipe-wall viscoelastic rheological behaviour; Tijsseling (1993), Tijsseling *et al.* (1996) and Tijsseling (1996) analysed fluid-structure interaction and cavitation; Covas *et al.* (2004a) and Ramos *et al.* (2004) considered pipe-wall viscoelasticity in combination with unsteady friction; Hachem & Schleiss (2012) analysed longitudinal stiffness heterogeneity by means of the combination of aluminium and PVC pipe reaches in an experimental set-up; and Keramat (2012) combined fluid-structure interaction, column separation and unsteady friction in a viscoelastic pipe.

The current paper aims at presenting and discussing experimental evidences of different features of fluid-structure, friction, and pipe-wall viscoelasticity during hydraulic transients carried out in three experimental set-ups assembled at the Laboratory of Hydraulics and Environment (LHE/IST) of Instituto Superior Técnico, Lisbon, Portugal. First, a straight copper pipe is tested for different support setups and discharges. Second, a coiled copper pipe is assessed and fluid-structure interaction due to the coil geometry is analysed. Finally, a polyethylene coiled pipe is tested, clearly showing the dominant effect of the pipe-wall viscoelasticy.

The key innovative features of this paper are: (i) the comparison of different pressure traces collected in three pipe-rigs with different configurations (straight and coiled) and pipe materials (metal and plastic), under the same controlled laboratory conditions, complemented with (ii) the physically-based discussion, supported on bibliographic references, of different phenomena affecting and dominating waterhammer in each case.

2 EXPERIMENTAL DATA COLLECTION

2.1 Copper straight pipe

A copper straight pipe (CSP) rig has been assembled at LHE/IST. The system is composed of a 15.49 m pipe, with an inner diameter, D, of 0.020 m and pipe-wall thickness, e, of 0.0010 m. Anchorages throughout the pipe constrain the longitudinal movement of the pipe system. Young's modulus of elasticity and Poisson ratio of the copper material were experimentally determined by measuring stress-strain states over a pipe sample for the experimental range of pressures. The obtained experimental values were the Young's modulus of elasticity E = 105 GPa and the Poisson ratio μ = 0.33. At the upstream end, there is a storage tank followed by a pump and an air vessel, and at the downstream end, there is a ball-valve pneumatically operated that allows the generation of fast transient events.

Three pressure transducers (WIKA S-10) were installed at the upstream, midstream and downstream positions of the pipe (PT1, PT2 and PT3). Strain gauges (TML FLA-2-11) disposed in the axial and circumferential directions (SG1 and SG2) were installed at the midstream and the downstream end of the pipe. The sampling frequency was 750 Hz for both pressure and strain measurements and 2400 Hz for wave celerity estimation. The initial discharge was measured for steady state conditions by a rotameter located downstream of the valve. Fig. 1 shows a schematic and a picture of the experimental set-up, with the location of the pressure transducers (PT).

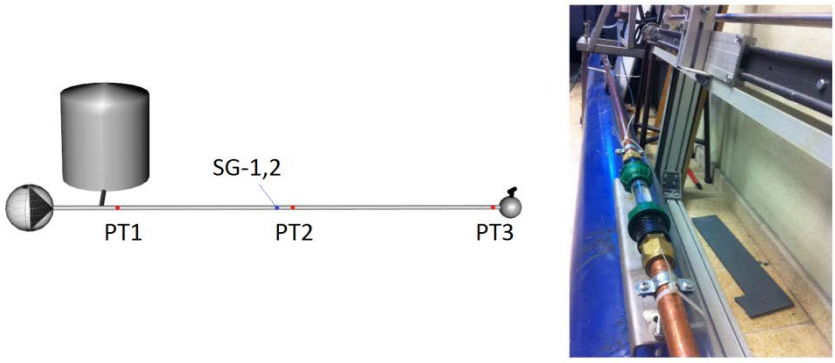

Fig. 1: Simplified schematic and view of the copper straight pipe.

Table 1 summarizes a set of tests carried out in this experimental set-up, characterized by the initial flow velocity and Reynolds number, the initial piezometric head and the maximum and minimum piezometric heads measured at immediately upstream the valve. Figs. 2 and 3 depict the transient pressure traces at the downstream and the midstream pipe locations corresponding to the tests carried out at the straight copper pipe.

Table 1: Characteristics of the straight copper pipe (CSP) tests.

Test ID	V_0 (m/s)	Re_0	H_0 (m)	H_{max} (m)	H_{min} (m)
CSP01	0.25	4931	45.36	75.62	15.27
CSP02	0.35	6930	44.87	85.15	4.90
CSP03	0.43	8542	44.67	93.68	-3.42

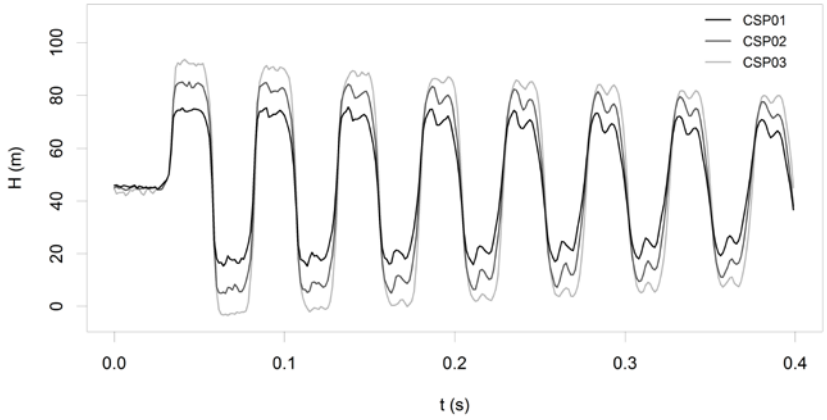

Fig. 2: Measured pressure data at the downstream boundary location for the waterhammer tests carried out at the straight copper pipe.

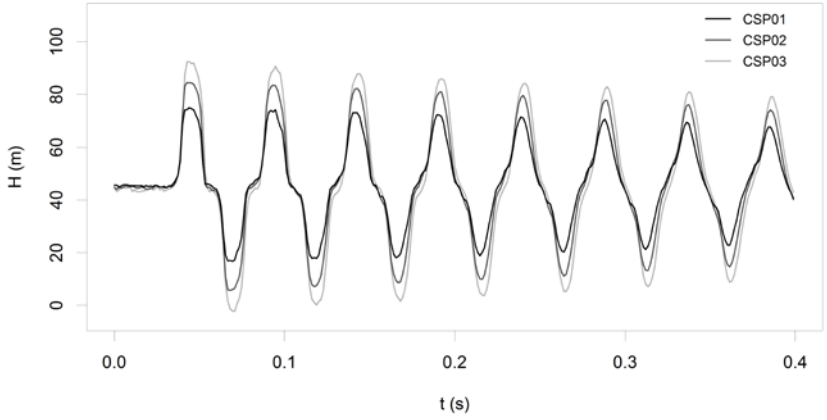

Fig. 3: Measured pressure data at the midstream boundary location for the waterhammer tests carried out at the straight copper pipe.

2.2 Copper coil pipe

The copper coil pipe (CCP), also assembled at LHE/IST, has an inner diameter, D, of 0.020 m, a pipe-wall thickness, e, of 0.0010 m and a pipe length, L, of 105 m. The torus

radius, R, is 0.45 m, its elevation is 1 m and 36 rings compose the entire coil. Each coil ring is fixed by 4 anchoring points disposed at 90° and with rubber supports. Similarly to the CSP facility, the value of Young's modulus of elasticity is E = 105 GPa and Poisson ratio μ = 0.33. Three pressure transducers (WIKA S-10) were located at the upstream, midstream and downstream positions of the pipe (PT1, PT2 and PT3). Strain gauges (TML FLA-2-11) disposed in the axial and circumferential directions (SG1 and SG2) were installed in the midstream location. The sampling frequency was 1000 Hz. The upstream and downstream conditions are similar to the ones in the CSP: there is a tank, a pump and an air vessel at the upstream end and a spherical valve to generate the transient events at the downstream end.

Fig. 4 shows a schematic and an overall view of the facility, with the location of the transducers.

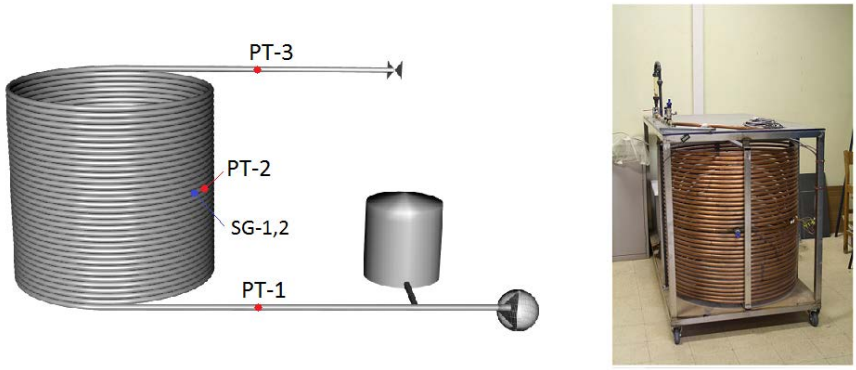

Fig. 4: Schematic and photograph of the copper pipe coil facility.

Table 2 shows a summary of a set of tests carried out in this experimental set-up according to the initial flow velocity, Reynolds number and the initial piezometric head at the downstream boundary before the valve closure, and maximum and minimum piezometric heads measured during the tests. Transient events were generated by a manual valve closure.

Table 2: Characteristics of the copper coil pipe (CCP) tests.

Test ID	V_0 (m/s)	Re_0	H_0 (m)	H_{max} (m)	H_{min} (m)
CCP01	0.09	1765	40.71	49.56	32.26
CCP02	0.18	3530	39.83	57.94	23.02
CCP03	0.35	7059	37.92	74.39	5.18

Figs. 5 and 6 depict the transient tests carried out in the copper coil pipe with transient pressures measured at the downstream and the midstream pipe locations.

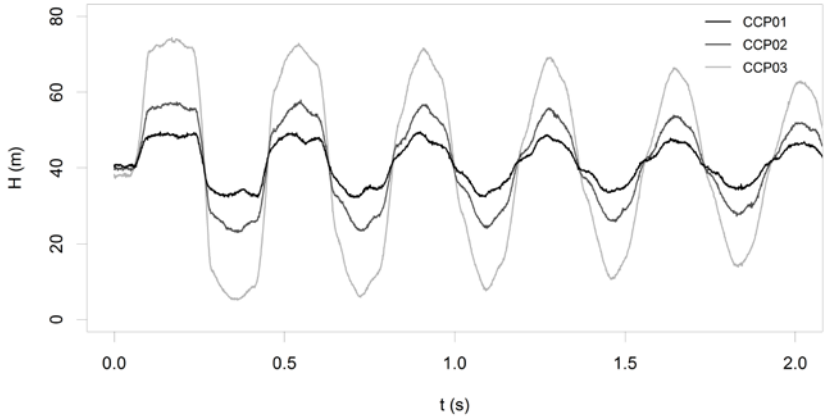

Fig. 5: Measured pressure data at the downstream boundary location for the waterhammer tests carried out at the copper coil pipe.

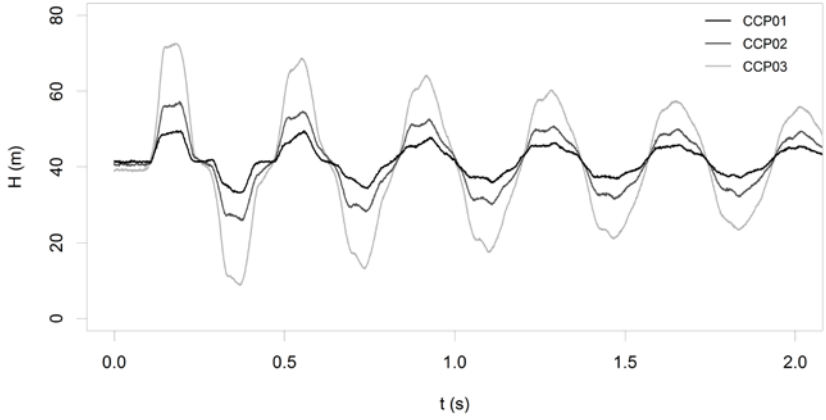

Fig. 6: Measured pressure data at the midstream boundary location for the waterhammer tests carried out at the copper coil pipe.

2.3 Polyethylene coil pipe

The polyethylene coil pipe (PECP), assembled at LHE/IST, is composed of two pipe coils of high density polyethylene (HDPE), with a total length, L, of 203 m, an inner diameter, D, of 0.043 m, a pipe-wall thickness, e, of 0.0030 m and a torus diameter, R, of 0.70 m. The coil structure is fixed by four braces disposed at 90°, linking the coil rings up and attaching them at the floor. The Young's modulus of elasticity and the wave speed

were previously assessed, for this set-up, by Soares *et al.* (2009), who after an inverse method estimated a Young's modulus E = 1.42 GPa and a wave speed a = 315 m/s. The theoretical Poisson ratio for polyethylene is $\mu = 0.43$. At the upstream end an air vessel is connected in series and at the downstream end a manual spherical valve allows the generation of transient events. Two pressure transducers (WIKA S-10) were located at the midstream and downstream positions of the pipe (PT1 and PT2). Strain gauges (TML FLA-2-11) were disposed in the midstream and in the axial and circumferential directions (SG1 and SG2). The sampling frequency was 50 Hz.

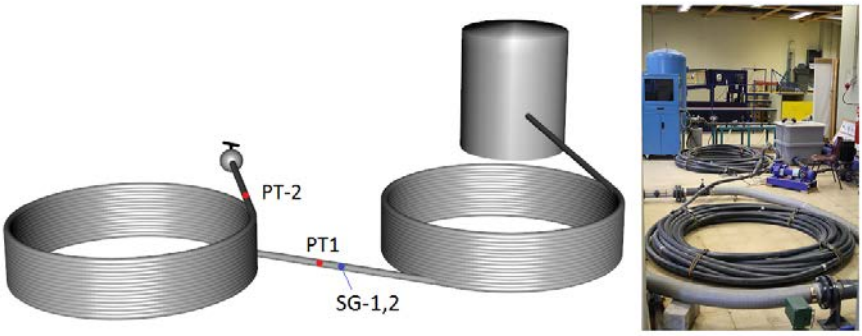

Fig. 7: Schematic and view of the polyethylene pipe coil facility.

Table 3 shows a summary of the tests carried out in the experimental set-up according to the initial flow velocity, Reynolds number and the initial piezometric head before the valve closure, and maximum and minimum piezometric heads measured at the valve during the assessed transient events.

Table 3: Characteristics of the polyethylene coil pipe (PECP) tests.

Test ID	V_0 (m/s)	Re_0	H_0 (m)	H_{max} (m)	H_{min} (m)
PECP01	0.20	8664	31.08	36.21	27.31
PECP02	0.33	14440	30.09	38.56	24.44
PECP03	0.46	20216	32.35	43.98	25.12
PECP04	0.72	31767	29.95	50.02	20.28
PECP05	1.05	46207	25.55	55.48	15.20

Figs. 8 and 9 depict the transient pressures at the downstream and midstream pipe locations measured during the waterhammer events corresponding to the tests at the polyethylene pipe coil.

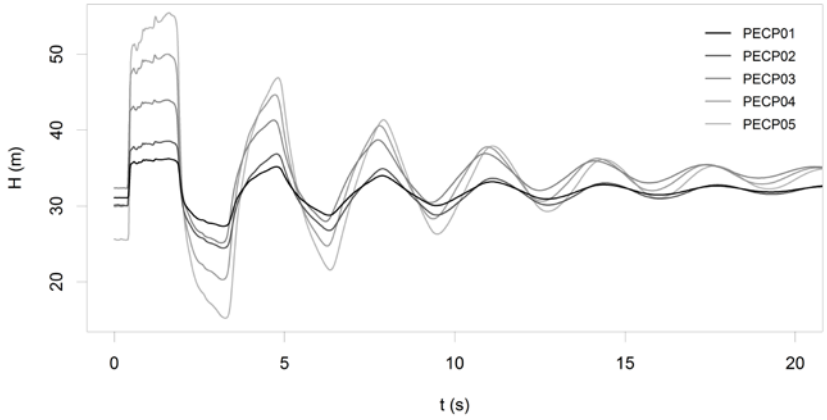

Fig. 8: Measured pressure data at the downstream boundary location for the waterhammer tests carried out at the polyethylene coil pipe.

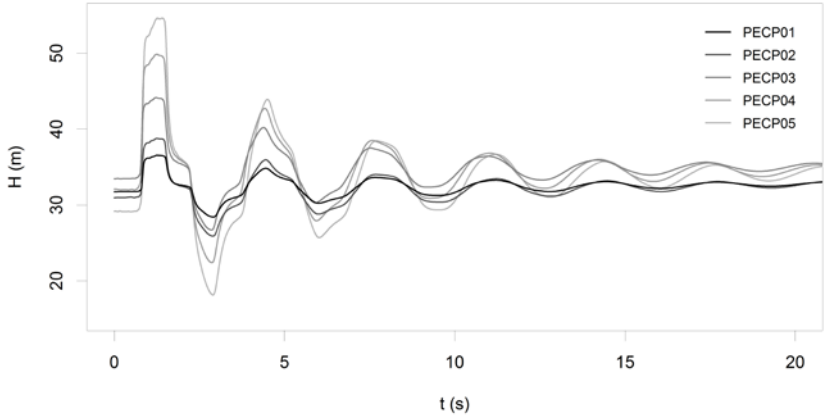

Fig. 9: Measured pressure data at the downstream boundary location for the waterhammer tests carried out at the polyethylene coil pipe.

3 EXPERIMENTAL EVIDENCE ANALYSIS

3.1 Pressure data analysis

The figures presented in the Section 2 (Figs. 2, 3, 5, 6, 8 and 9) have already shown how differently transient events propagate throughout the three experimental set-ups,

generated for similar steady state conditions (i.e., initial Reynolds numbers) and by fast valve manoeuvres (though with different rates of closure). Differences of piezometric heads and time scales between the transient events measured in each rig hinder a straightforward comparison. Dimensionless pressure traces are necessary to facilitate the comparison between systems' responses in terms of amplitude, dispersion and shape of the transient wave.

Observed transient pressure wave periods and amplitudes are associated with two main characteristics of the pipe system – the wave celerity, *a*, and the pipe length, *L* – and one with the flow conditions – the initial steady state velocity, *Vo*.

The *wave period*, *T*, depends only on the ratio between pipe length and wave celerity – Equation (1) – and is, therefore, independent of the initial conditions; it is a physical property of the pipe system (pipe elasticity, inner diameter, wall thickness and constraint conditions) together with the fluid (compressibility).

$$T = \frac{4L}{a} \tag{1}$$

The *maximum pressure rise*, ΔH_{JK}, described by the Joukowsky formula – Equation (2) – depends not only on the pipe and fluid physical properties, but also on the initial flow conditions and the gravitational acceleration, being proportional to the product between the initial flow velocity V_0 and the wave celerity *a*.

$$\Delta H_{JK} = \frac{aV_0}{g} \tag{2}$$

Fig. 10 depicts the dimensionless plots of transient pressure traces for selected tests from each facility. The tests were selected with the aim to analyse transient flow free of cavitation but energetic enough to excite and depict the piping structural behaviour. These have been drawn by first subtracting measured head by the initial pressure head, and then by dividing by Joukowsky overpressure (ΔH_{JK}); and, on the other side, by dividing the time axis by the wave periods presented in Table 4. Wave celerity values have been empirically estimated by comparing the time lag between pressure measurements at the downstream and midstream pipe positions. Presented values correspond to averaged values from all the tests carried out in each facility; minor discrepancies lower than 1% have been observed.

Table 4: Main properties of the assessed tests.

Test ID	a (m/s)	T (s)	V_0 (m/s)	ΔH_{JK} (m)	t_{valve} (s)
CSP03	1260	0.053	0.43	48.85	0.003
CCP03	1193	0.384	0.35	36.5	0.025
PECP03	315	2.88	0.46	13.2	0.050

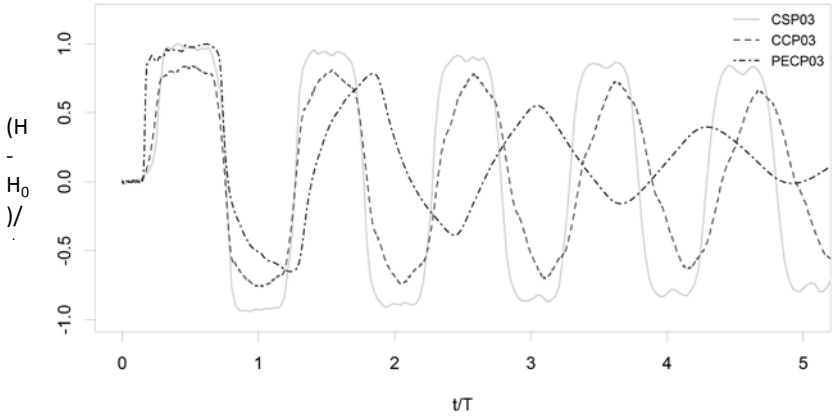

Fig. 10: Dimensionless transient pressures in the three set-ups.

Figure 10 shows different attenuation, shape and phase shift of transient pressure responses of each experimental set-up. The pressure trace in the straight copper pipe facility is the one that approaches the most to the theoretical "squared" wave shape described by the classic waterhammer theory. This is not only due to the very fast valve closure (almost instantaneous), but also due to the linear elastic rheological behaviour of the pipe wall and the straight pipe configuration; however, reflection appears in the pressure trace. Transient pressure in the polyethylene pipe shows an extremely higher damping, shape change and time delay of the transient pressure wave, typical of viscoelastic pipes (Covas, 2004b and Covas, 2005). The wave measured in the copper coil system seems to be in between the two previous ones.

Wave dissipation

With regards to the wave attenuation, the copper straight pipe is the one with the lowest transient pressure wave damping, and the one used for comparison. This is due to three main reasons. The first is that steady and unsteady friction losses are less important in this pipe system due to its small length (*ca*. 15 m) in comparison with the two pipe coils (copper coil L=115 m and PE coil L= 200 m). The less the pressure wave travels, the lower the frictional damping is during the transient event. The second reason is the pipe having a linear elastic behaviour, deforming instantaneously with pressure changes, without a retarded response. The third reason is the pipe being straight and well-fixed to the supporting structure with an almost a motionless downstream valve, whereas the other two rigs are pipe coils subjected to a high FSI effects as explained in the following paragraphs.

The first pressure peak in the copper pipe coil is 15 to 20% lower than the Joukowsky overpressure, which corresponds to $(H-H_0)/\Delta H_{JK} = 1$ in Fig. 10. The main reason for this reduction is the particular feature of FSI occurring in the pipe coil individual rings: during the transient propagation, pipe rings have a "breathing effect" as they expand axially and radially for positive pressures increasing the pipe inner volume and, consequently, attenuating the pressure peaks, and *vice-versa* for negative pressures; this

attenuation is particularly evident in the first pressure rise. This phenomenon has been comprehensively analysed by Ferras *et al*. (2015).

Finally, the viscoelastic response of the HDPE pipe has also a crucial contribution to the wave attenuation (Covas, 2004b and Covas, 2005). Despite the "breathing effect" occurring also in the PE pipe, this is less evident in the pressure wave as the wave dissipation is dominated by the viscoelastic behaviour of the pipe wall characterised by an instantaneous elastic response followed by a retarded viscous response (Covas, 2004b).

Wave shape

Some aspects might be pointed out regarding the wave shape. The waterhammer wave in the copper straight pipe is the closest to the theoretical "squared" wave for the basic classic assumptions. However, a reflection, which develops in every wave cycle, can be observed in the form of a pressure drop in each peak (Fig. 10, grey line). The cause of this effect is associated to FSI; further investigation is being carried out in this respect.

On the other side, clearly a different wave shape is observed in the copper coil facility (in comparison to the straight pipe) which is associated with two phenomena. The first is friction that, as explained, is more evident in the coil system due to a higher length and a larger inertia of the water column. The second is the coil rings movement that directly induces FSI despite the existing four fixing supports at 90° spacing.

Regarding the PE facility, an evident shape change is noticed, both in the first pressure peak and throughout the wave propagation. The pressure rise in the first peak is associated to the line packing effect is more evident in the PE facility; this effect is dependent on the head losses gradient during the initial steady state, which is higher in test carried out in the polyethylene pipe (which has a higher Re). The wave shape changes during its propagation are mainly due to the retarded response of the HDPE material which has a viscoelastic rheological behaviour (Covas et al., 2004, 2005). Unsteady friction may also contribute to this delay, however the relative importance of these two physical processes to wave shape changes merits further investigation. Additionally, a relatively much faster valve manoeuvre is observed, as the slope of the first pressure rise is much steeper in the polyethylene case; although having the slowest valve closure, the wave propagates one third slower than in the copper and, in addition, the pipe is the longest, resulting in an apparent fast manoeuvre when plotted in dimensionless terms.

Wave delay

Regarding the wave timing, a smooth delay can be observed in the coil copper facility in comparison to the straight pipe, and a much more evident delay in the case of the polyethylene coil. In the case of the copper coil system, the time delay suggests both steady and unsteady friction affect the pressure signal more than in the straight pipe: this is associated to the pipe much higher length.

With regard to the polyethylene set-up, the reason of such delay is mainly attributed to the retarded response of the pipe-wall. In viscoelastic pipes, maximum or minimum pressure fluctuations are rapidly attenuated and the overall transient pressure wave is delayed in time due to the retarded deformation of the pipe-wall (Covas, 2004b).

3.2 Strain data analysis

In addition to pressure measurements, the collected strain data allows the analysis of the rheology and the structural displacements of the pipe systems during the transient tests. Figs. 11, 12 and 13 depict circumferential stress *vs.* circumferential strain, where stress is computed from the pressure signal by Eq. 3, both in the straight pipe and in the pipe coils (Ferras *et al.* 2014).

$$\sigma_c = \frac{pD}{2e} \tag{3}$$

The circumferential strain measurements are corrected (ε_c') using Eq. 4, which is derived from the extended Hooke's law for isotropic materials. This correction allows for an explicit definition of circumferential strain independent from the axial strain.

$$\varepsilon_c' = \frac{\varepsilon_c + \nu\varepsilon_a}{1 - \nu^2} \tag{4}$$

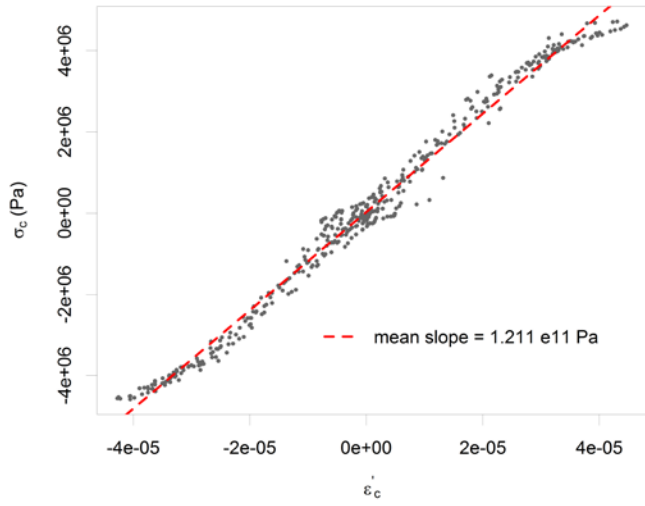

Fig. 11: Circumferential stress *vs.* circumferential strain during the transient test CSP03.

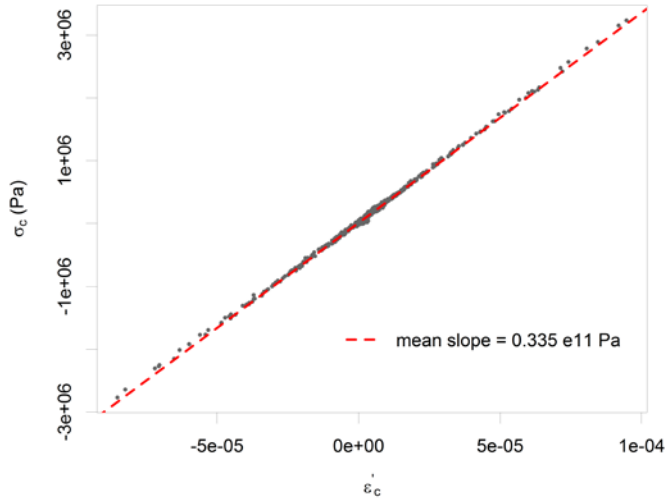

Fig. 12: Circumferential stress *vs.* circumferential strain during the transient CCP03

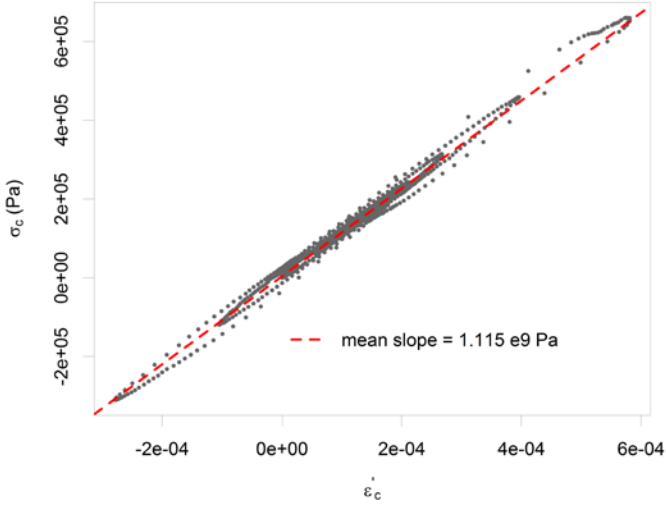

Fig. 13: Circumferential stress *vs.* circumferential strain during the transient test PECP03.

The strain plots of Figs. 11, 12 and 13 give important information on the mechanical behaviour of the pipe systems. Fig. 12 shows a clear linear-elastic behaviour of the pipe-

wall material in the copper coil facility, as the measurements in the stress-strain space are presented in a straight line. Greater scatter can be observed in Fig. 11, corresponding to the stress-strain cycles during the transient event in the copper straight pipe facility. The reasons for this scatter are: collected data in the straight copper pipe are more affected by noise especially in the steady state region (see Fig. 2,); and the supporting structure and the valve fixing structure have a direct impact on observed transient pressures. On the other side, in the case of the stress-strain plot for the polyethylene facility (Fig. 13), different loading and unloading paths can be distinguished, typical of the *hysteretical behaviour* of the PE pipe-wall material. This phenomenon has been extensively analysed and reported by Covas (2003) and Covas et al. (2004).

The ratio between stress and strain is the Young's modulus of elasticity, an intrinsic property of the pipe material that is affected by temperature, stress-strain history and aging (Ashby and Jones, 1994; Ward and Sweeney, 2012). In this context, the main slope of the trend-line fitted to collected data in Figs. 11, 12 and 13 should give some insight about the Young's modulus of the respective pipes. For instance, the slope of the straight copper pipe in Fig. 11 (121 GPa) is quite close to the theoretical Young's modulus of the copper material (E = 105 GPa). However, this is not always the case.

In the HDPE coil (Fig. 13), the observed slope (E = 1.12 GPa) is higher than the one suggested by the pipe manufacture (1 GPa) but lower than the Young modulus calibrated by Soares *et al.* (2009) (E = 1.42 GPa). On the one hand, the obtained slope corresponds to the static Young modulus of elasticity of the PE (*ca.* 1 GPa), whereas the observed by Soares corresponds to the dynamic Young modulus, about 1.5 times the static one for PE. On the other hand, tests presented in this paper have been carried out 8 years after the ones from Soares *et al.* (2009) and the material has aged and become stiffer (this justifies the increase of Young modulus from 1 to 1.12 GPa). Despite being inside the laboratory building, the pipe coil has been continuously exposed to temperature changes, humidity and indirect sun radiation, which have definitively affected its mechanical properties (Ward and Sweeney, 2012; Covas et al., 2004)

In the case of the copper coil piping system, the mean slope in Fig. 12 (E= 33 GPa) substantially differs from the expected Young's modulus, which should be of the magnitude the one from Fig. 11 (121 GPa) as the material and pipe cross-section is the same. The reason is a pipe cross-sectional bending (Ferras *et al.*, 2014). In the coiled pipe the cross-section is not circular but a bit elliptic. This ellipticity varies in function of the inner pressure load and consequently circumferential strain measurements are distorted.

4 CONCLUSIONS

This paper summarises physical observations of transient pressures in three different experimental facilities: a copper straight pipe, a copper pipe coil and a high-density polyethylene pipe coil. Hydraulic transient tests were generated by fast downstream valve closures for different initial steady state conditions. Both transient pressures and circumferential and axial strains were measured at the downstream and at the midstream pipe positions.

Several distinct damping phenomena have been identified, which affect the attenuation, shape and timing of the pressure wave, namely, friction, fluid-structure interaction and pipe-wall viscoelasticity. The transient wave in the straight copper pipe has shown to be

the least affected by FSI, while the mechanical behaviour of the PE pipe has proven to significantly affecting the dissipation, shape and phase of the transient pressure wave.

Despite being the closest to the theoretical waterhammer waves, the waves generated in the copper straight pipe present a reflection in each wave cycle due to FSI in the intermediate supports and at the valve section. Nonetheless, their squared cyclic signal with low damping has been used as a reference to compare the other two facilities.

For similar initial steady state conditions and dimensionless closure times, the copper coil pipe system presents a much different mechanical behaviour. Higher head losses increase the wave attenuation. Fluid-structure interaction by the transient wave loading the rings and radially deforming them one by one all throughout the coil change the wave shape, and a time delay is observed in the wave propagation. The corresponding stress-strain relationship illustrates such FSI (Fig. 12), characterized by a rigorous linear-elastic behaviour of the pipe-wall material, where the slope of the loading-unloading cycles differs substantially from the theoretical Young's modulus of elasticity.

Finally, a clear viscoelastic rheological behaviour is observed in the polyethylene facility through a characteristic shape change of the wave and its very fast attenuation. This viscoelastic behaviour can be noticed in the stress-strain plot (Fig. 13), in which *hysteresis* is manifested through different paths in the loading-unloading curves on the stress-strain space. Nevertheless, the average slope of the stress-strain curves (the static E_0) is lower than the observed Young's modulus of elasticity by Soares *et al.* (2009) (the dynamic E_0) but not as low as expected (*i.e.* the ratio between the dynamic/static E_0's equal to 1.5). The reason is the aging of the polyethylene material that has made it stiffer now than it was before, increasing its static Young's modulus of elasticity.

The experimental evidence presented herein is being used to develop, calibrate and validate numerical models to simulate complex hydraulic transients, including fluid-structure interaction and pipe viscoelasticity, objects of other communications and research papers.

ACKNOWLEDGEMENTS

This research is supported by the Foundation for Science and Technology (FCT, Portugal) through the project ref. PTDC/ECM/112868/2009. The first author is funded by the PhD grant ref. SFRH/BD/51932/2012 also issued by FCT under IST-EPFL joint PhD initiative. The second author is funded by the Swiss Competence Centre for Energy Research – Supply of Electricity (SCCER-SoE, Switzerland).

REFERENCES

Ashby, M. F., and Jones D. (1994). *Engineering materials*. Pergamon press.

Bergant, A., Tijsseling, A. S., Vítkovsky, J. P., Covas, D. I., Simpson, A. R. & Lambert, M. F. (2008). Parameters affecting water-hammer wave attenuation, shape and Timing. Part 1: Mathematical tools. *Journal of Hydraulic Research* 46(3), 373-381.

Chaudhry, H. M. (2014). *Applied hydraulic transients*. Springer New York.

Covas, D., Ramos, H., Graham, N., Maksimovic, C. (2004a). The interaction between viscoelastic behaviour of the pipe-wall, unsteady friction and transient pressures. *BHR Group, Proc. of the 9th Int. Conf. on Pressure Surges, Chester, UK*, p. 760.

.

Covas, D., Stoianov, I., Ramos, H., Graham, N., & Maksimovic, C. (2004b). The dynamic effect of pipe-wall viscoelasticity in hydraulic transients. Part I - Experimental analysis and creep characterization. *Journal of Hydraulic Research*, 42(5), 517-532.

Covas, D., Stoianov, I., Mano, J. F., Ramos, H., Graham, N., & Maksimovic, C. (2005). The dynamic effect of pipe-wall viscoelasticity in hydraulic transients. Part II—Model development, calibration and verification. *Journal of Hydraulic Research,* 43(1), 56-70.

Ferràs, D., Covas, D. and Schleiss A. (2014). Stress–strain analysis of a toric pipe for inner pressure loads. *Journal of Fluids and Structures* 51: 68-84.

Ferràs, D., Covas, D. and Schleiss, A. (2015). Comparison of conceptual models for fluid-structure interaction in pipe coils during hydraulic transients. *Journal of Hydraulic Research* (*submitted*).

Hachem, F. E., & Schleiss, A. J. (2012). Effect of drop in pipe wall stiffness on water-hammer speed and attenuation. *Journal of Hydraulic Research,* 50(2), 218-227.

Keramat A. (2012). Waterhammer with column separation, fluid-structure interaction and unsteady friction in a viscoelastic pipe. *BHR Group, Proc. of the 11th Int. Conf. on Pressure Surges, Lisbon, Portugal*, pp. 443-460.

Krause, N., Goldsmith, W. & Sackman, J. (1977). Transients in tubes containing liquids. *International Journal of Mechanical Sciences* 19(1), 53-68.

Ramos, H., Covas, D., Borga, A. & Loureiro, D. (2004). Surge damping analysis in pipe systems: modelling and experiments. *Journal of Hydraulic Research* 42(4), 413-425.

Soares, A. K., Covas, D. I., Ramos, H. M., & Reis, L. F. R. (2009). Unsteady flow with cavitation in viscoelastic pipes. *International Journal of Fluid Machinery and Systems*, 2(4), 269-277.

Stuckenbruck, S. & Wiggert, D. (1986). Unsteady flow through flexible tubing with coupled axial wall motion. *BHR Group, Proc. of the 5th International Conference on Pressure Surges, Hannover Germany*, pp. 11-17.

Tijsseling, A. (1996). Fluid-structure interaction in liquid-filled pipe systems: a review. *Journal of Fluids and Structures* 10(2), 109-146.

Tijsseling, A., Vardy, A. & Fan, D. (1996). Fluid-structure interaction and cavitation in a single-elbow pipe system. *Journal of Fluids and Structures* 10(4), 395-420.

Tijsseling, A. S. (1993). *Fluid-structure interaction in case of waterhammer with cavitation*. Ph.D. thesis, TU Delft, Delft University of Technology.

Walker, J. & Phillips, J. (1977). Pulse propagation in fluid-filled tubes. *Journal of Applied Mechanics* 44(1), 31-35.

Ward, I. M., and Sweeney J. (2012). *Mechanical properties of solid polymers*. John Wiley & Sons.

Weijde, P. V. D. (1985). Prediction of pressure surges and dynamic forces in pipeline systems, influence of system vibrations on pressures and dynamic forces (fluid structure interaction). In: *Transactions of the Symposium on Pipelines, Utrecht, The Netherlands.*

Williams, D. (1977). Waterhammer in non-rigid pipes: precursor waves and mechanical damping. *Journal of Mechanical Engineering Science* 19(6), 237-242.